J. Water Environ. Nanotechnol., 6(3): 252-264 Summer 2021

ORIGINAL RESEARCH PAPER

Structural, Optical, Thermal, Magnetic Properties of Zirconia Nano-rods and their Photocatalytic and Antimicrobial Properties

Jeba Rengaswamy [1,4,*], Radhika Sathasivam [2,4], Padma Chellaia Muthammal [3,4], Ascar Davix Xavier Durai [5]

[1] Research Scholar, Reg.No:18223282132002, Women's Christian College, Tamilnadu, India-629001
[2] Department of Physics, Pioneer Kumaraswamy College, Tamilnadu, India- 629003
[3] Department of Physics, Women's Christian College, Tamilnadu, India-629001
[4] Affiliated to Manonmaniam Sundaranar University, Abishekapatti, Tirunelveli, India- 627012
[5] Department of Electronics and Communication Engineering, R.V.R. & J.C. College of Engineering, Andhra Pradesh, India - 522019

Received: 2021-5-07 Accepted:2021-06-19 Published: 2021-07-01

ABSTRACT

Multifunctional Zirconia Nanorods performing photocatalysis, anti-bacterial and anti-fungal activities are presented in this article. Tetragonal Zirconia is synthesized by the simple co-precipitation method. The synthesized Zirconia is characterized by various characterization methods such as XRD, SEM, EDX, UV-Vis, PL, VSM, and TG/DTA analysis. Exploration of powder XRD pattern indicates tetragonal phase. SEM image illustrates rod-shaped morphology. UV-Vis spectra reveal that the synthesized catalyst has a wide bandgap of about 4.6eV. The emission peaks in the PL spectra reveal the presence of oxygen vacancies in the sample. Room Temperature Ferromagnetism (RTFM) is confirmed from VSM measurements. The performance of Zirconia nanorods in various applications such as photocatalysis, anti-bacterial and anti-fungal activities has been analyzed. t-ZrO_2 photocatalyst degrades methylene blue dye with 80% removal efficiency in 180 minutes under UV light irradiation. t-ZrO_2 obtained a 28mm inhibition zone against *Staphaureus* for anti-bacterial assessment while Amikacin has 15mm inhibition and obtained 25mm inhibition zone against *Candida Albicans* for anti-fungal assessment while Nystatin has 20mm inhibition. t-ZrO_2 shows a superior inhibiting effect against both gram-positive and gram-negative bacterial pathogens. Owing to its high surface area it exhibits the greatest inhibiting effect against fungal strain.

Keywords: *Co-precipitation, Tetragonal, Room Temperature Ferromagnetism.*

How to cite this article
Jeba R., Radhika S. , Padma C.M., Ascar Davix X. Structural, Optical, Thermal, Magnetic Properties of Zirconia Nano-rods and their Photocatalytic and Antimicrobial Properties. J. Water Environ. Nanotechnol., 2021; 6(3): 252-264.
DOI: 10.22090/jwent.2021.03.006

INTRODUCTION

Nano-structured materials fascinate greater intentness through various fields because of their physical and chemical properties. Metal oxide nanomaterials offer industrial and biomedical applications. Among metal oxide nanoparticles Zirconium oxide (ZrO_2), often called Zirconia, is a peculiar candidate because of its unique properties such as high dielectric constant, low melting point, low electrical conductivity, wide bandgap, and environmentally sound on comparing with other ceramic oxides [1-3]. Zirconia is extensively used as a catalyst in diverse applications [4].

Owing to the hasty evolution of textile industries discharge of excess dyes pollute natural water bodies which may produce a harmful effect on both human and aquatic life. Numerous nano-

* Corresponding Author Email: *jeba170787@gmail.com*

sized metal oxides such as titanium oxide, tin oxide, iron oxide have been explored for photocatalysis which may disintegrate excess dyes. Among the various photocatalysts, ZrO2 is an optimistic material to perform photocatalysis due to its high negative CB potential, acid-base property, oxidation-reduction ability, and cost-effectiveness [5-8]. Only a few previous reports show the photocatalytic degradation of pollutants using pure ZrO2 nanoparticles [38,39].

Nano-sized materials have antimicrobial properties along with physical and chemical properties [9]. Nano zirconia has high surface energy and has good chemical reactivity that causes superior anti-bacterial and anti-fungal properties [10, 11]. Previous studies about nano zirconia exhibit the anti-bacterial and anti-fungal consequences on C. Albicans and Aspergillusniger [12]. Active oxygen species formed from nano zirconia may improve the anti-bacterial activity due to the interruption of the cell membrane of microorganisms with nano zirconia. Higher permeability of the cell membrane results in the accumulation of nano zirconia in the cell membrane and cytoplasmic region of the cells [13]. Nano-sized ZrO_2 interferes with cell function and deforms the fungal hypha. Thus it exhibits a superior inhibiting effect against the growth of fungal strains [14,15]. When the particle size is reduced, the surface area-to-volume ratio increases. Due to their high surface-area-to-volume ratio and unique physical and chemical properties, nano zirconia has generated anti-microbial agents against bacterial and fungal strains.

Different physical and chemical techniques have been used for the synthesis of ZrO_2 nanoparticles including molten salt synthesis, sol-gel synthesis, hydrothermal synthesis, and co-precipitation methods [16,17]. Among these techniques co-precipitation is an attractive method on account of the production of smaller size materials with good quality, the process of simplicity, narrow particle size distribution, less agglomeration, and cost-effectiveness [18,19]. Present work focuses on the synthesis of tetragonal zirconia by simple co-precipitation method and makes it perform a variety of functions including photocatalysis, antibacterial and antifungal effects. Many researchers have reported the synthesis of monoclinic phase ZrO_2. We found few methods that deal with the degradation of MB dye and antimicrobial studies with tetragonal ZrO_2. Of particular interest to this issue, facile synthesis and characterization of tetragonal ZrO_2 are performed for the analysis of the degradation of MB dye and antimicrobial activities.

EXPERIMENTAL

Materials and preparation

Zirconium oxychloride, sodium hydroxide, and distilled water are the starting materials used for the preparation of ZrO_2 nanoparticles. Nano rods of pure ZrO_2 are prepared by the simple co-precipitation method. An aqueous solution of Zirconium oxychloride and sodium hydroxide are taken in the ratio of 0.5:2 M to maintain the pH 12. The aqueous solution of Zirconium oxychloride is stirred at 60°C using a magnetic stirrer. NaOH solution is added drop by drop till the pH value reaches 12 and stirred constantly for 2 hours at 60°C. The obtained precipitate is filtered and then washed with distilled water repeatedly and then finally with acetone to remove impurities. Thereafter the precipitate is dried at 150°C by using a hot air oven. After drying, the obtained precipitate is ground by using mortar and pestle to get a fine powder. This fine powder is calcined at 500°C by utilizing a muffle furnace to get a nanostructured Zirconia.

Catalyst characterization

The structural property of synthesized nano zirconia including crystallite size, phase identification has been confirmed using XPERT-PRO diffractometer in the diffraction angle 2θ range from 10° to 80 °. UV VIS spectrums for nano ZrO_2 have been recorded in the wavelength range of 100 to 1100nm using Perkin Elmer Lambda 35 spectrophotometer. The photoluminescence analysis is carried out by Fluorescence Spectrophotometer (Cary Eclipse) with an exciting wavelength of 270nm. The structural morphology and the chemical state are noticed with Scanning Electron Microscope (SEM) and energy dispersed X-ray (EDX) using EV018 (CARL ZEISS) and Quantax 200 with X Flash 6130. Lakeshore Vibrating Sample Magnetometer (VSM) measurements are recorded for the study of the magnetic properties of the prepared nanoparticles. Thermogravimetric (TG) and Differential Thermal Analysis (DTA) measurements are recorded using an exstar-6300 model thermal analyzer for the study of thermal characteristics of ZrO_2 nanoparticles under Nitrogen gas atmosphere.

Photocatalytic activity of synthesized ZrO_2

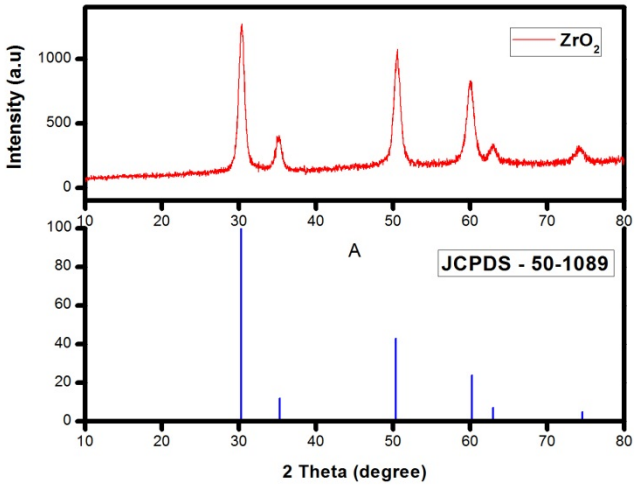

Fig. 1. XRD pattern of nano ZrO2

nanoparticles annealed at 500°C on the degradation of methylene blue (MB) is analyzed. An aqueous solution of methylene blue (0.1M, 50ml) was taken and 0.2g of photocatalyst is suspended in that solution. The experiment is done under UV light irradiation. The solution was exposed to a halogen lamp of 50W with continuous stirring. For every 60min, 4ml of dye solution was taken from the system and the dye removal efficiency is analyzed by UV-Vis spectrometer.

Kirby-Bauer test (KB test)

For the bacterial inhibition assay, the KB test otherwise known as disc-diffusion antibiotic sensitivity test was used. Nutriment agar media of pH 7.2 is prepared and inoculated with the experimenting organism for the growth of bacteria. A suspension of gram-positive and gram-negative bacteria is sprayed over the total area of antibiotic discs. Amikacin was used as a reference antibiotic which is also sprayed alongside the disc. The plate is then under incubation at 35°c for 16 hours [20]. Zones of bacterial inhibition develop in and around the sample. After incubation, the diameter of the inhibition zones is measured. Further antifungal activities of Zirconia rods were also determined against *candida Albicans* and *Candida parapsilosis* fungal strains by agar diffusion method, for which nystatin was used as reference antifungal. Zone of inhibition is the region in which the bacterial growth is terminated due to bacteriostatic consequence of the compound and it evaluates the inhibitory effect of the compound concerning a specific microorganism [21].

RESULTS AND DISCUSSION

Crystallographic analysis of Nano zirconia

The wide bandgap Zirconia nanorods are synthesized using the co-precipitation method and annealed at 500°C. The XRD pattern is used to identify the phase of synthesized nanoparticles and it is shown in Fig. 1. It confirms the pure tetragonal phase (JCPDS-50-1089) and it is indexed with standard peaks. The peaks are indexed as follows: 30.24° (011), 34.97° (002), 35.31° (110), 50.59° (112), 59.92° (013), 63.04° (202) and 74.34° (220). Also, no impurity peaks are identified. The diffraction pattern shows sharp and well-defined peaks which indicate the highly crystalline nature as well as purity of the sample [22]. From Full-Width Half Maximum (FWHM) of reflections of tetragonal zirconia, the average crystallite size (D) is calculated using Scherrer's formula, $D = \frac{0.9\lambda}{\beta \cos\theta}$, where, 'λ' is the wavelength of the X-rays; 'θ' is the Bragg's diffraction angle, and 'β' is the full width at half maximum (FWHM) of the diffraction peaks (in radians).

The calculated average crystallite size of the sample is found to be 29.74nm. The obtained crystallite size is small due to the presence of oxygen vacancies at the boundaries and the surface of grains. The existence of oxygen vacancies may stop the growth of nanoparticles and make a stress field. The dislocation density (δ) is the length of dislocation per unit volume which depends on the crystallite size (D) and it is

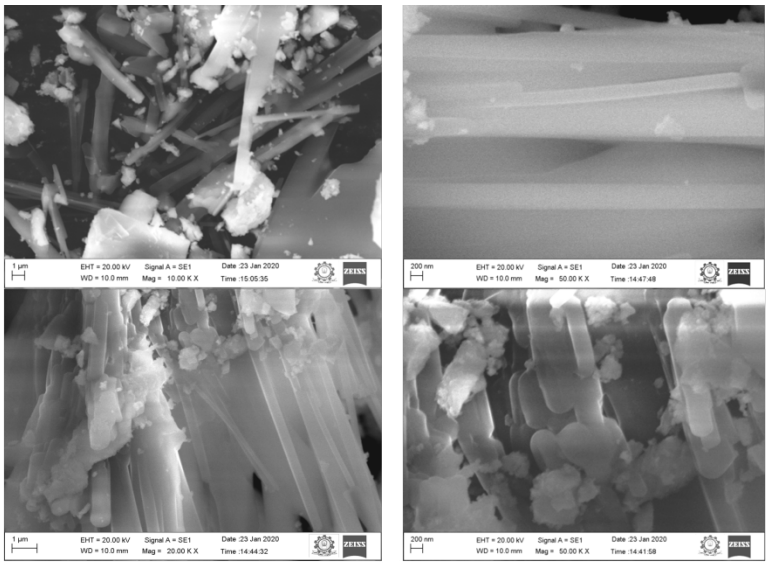

Fig. 2. SEM images of Zirconia with different magnifications

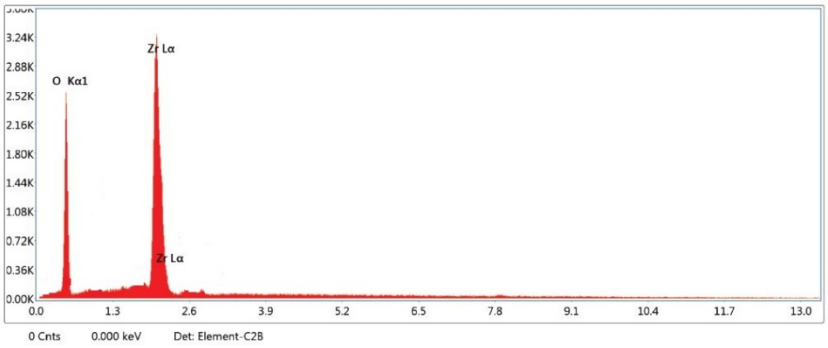

Fig. 3. EDX characterization spectra of ZrO2

calculated using the relation, $\delta = \frac{1}{D^2}$. The obtained dislocation density value is 1.23 × 10^{15} lines/m^2. During the deformation, the dislocation density increases beyond the elastic limit. The stacking fault probability is calculated using the formula $SF = \frac{2\pi^2}{45\sqrt{3}\tan\theta}$. Stacking disorder in the structure can be investigated using the SF value. It is used to localize the distribution of stacking faults. The obtained SF value is 0.486. The microstrain produced due to the dislocations in the nanoparticles is calculated using the relation, $\varepsilon = \frac{\beta\cos\theta}{4}$, where β is the FWHM and θ . is the diffraction angle. The obtained microstrain value is 1.26 × 10^{-3} which signposts better quality of deposited nanostructures. Microstrain decrease with an increase in hydrothermal treatment time and an increase in particle size. The increase of crystallite size and decrease of microstrain leads to the growth of particle size.

Morphology and chemical state of nano zirconia

The morphology of the synthesized ZrO_2 nanoparticle is analyzed with scanning electron microscopy (SEM). The SEM micrographs of t-ZrO_2 with different magnifications are shown in Fig. 2. It is observed that the morphology of the synthesized samples is rod shape. The obtained particle has a nano-sized structure and well-defined grains. Fig. 2 clearly shows that the rod-shaped zirconia nanoparticles are in uniform size and smooth surface. The EDX characterization dicts the elemental composition of the prepared ZrO_2nanoparticles. The EDX characterization spectrum is shown in Fig. 3. A high intense peak is identified for Zirconium (Zr) and Oxygen (O)

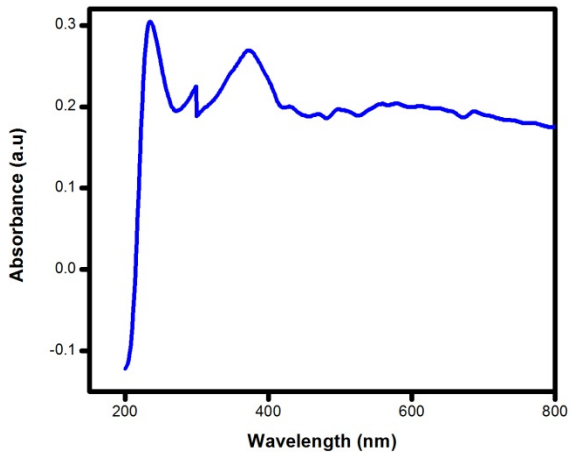

Fig. 4. Optical absorbance spectrum of ZrO2

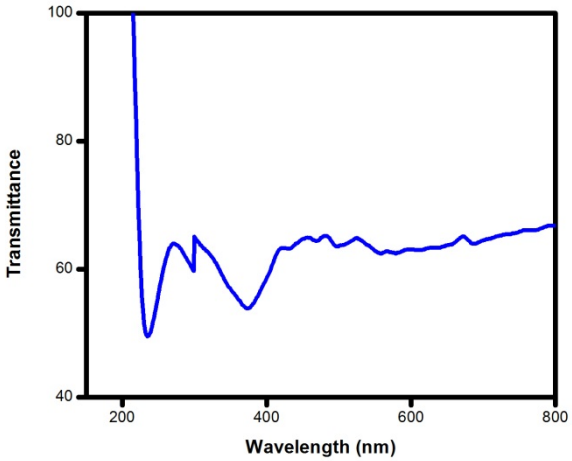

Fig. 5. Optical transmittance spectrum of ZrO2

elements.

Optical Investigation

The Optical absorbance and transmittance spectrum of ZrO_2 at 500°C annealing temperature are shown in Figs. 4 and Fig. 5. The strong absorption peak for ZrO_2 occurs at 235 nm and 371nm which is in the UV region. It is because of the excitation of an electron from the valence band to the conduction band due to the presence of conjugated pi-bonding systems and the surface defect states. The excitations of electrons due to the transition of ($O^{-2} \rightarrow Zr^{+4}$) cause the absorption peak in the absorption band [29]. There is a transition between the 2p energy state of O which is present in the valance band and the 4d (x^2-y^2, z^2) energy state of Zr which is present in the conduction band. In the visible region, there is no distinctive feature for d-d transition. It is due to the configuration of d0 in Zr^{4+} ions. Compared to the optical band gap for bulk ZrO_2 in the literature [30], the obtained absorption peak has lower energy. The reduction of nanoparticle size causes changes in the bandgap of the particle. The scattering centers and mechanical stress can be affected because of the variation in the band gap of the nanoparticle. The bandgap energy of the prepared sample is calculated by using Tauc relation,

$$\left(\alpha h\vartheta\right)^n = A\left(h\vartheta - E_g\right). \quad (1)$$

where $h\vartheta$. is the energy of the photon, E_g. is the bandgap energy, and A is the proportionality constant. n takes the value $1/2$. for direct allowed transitions and α is the absorption coefficient [23]. The absorption coefficient α is determined

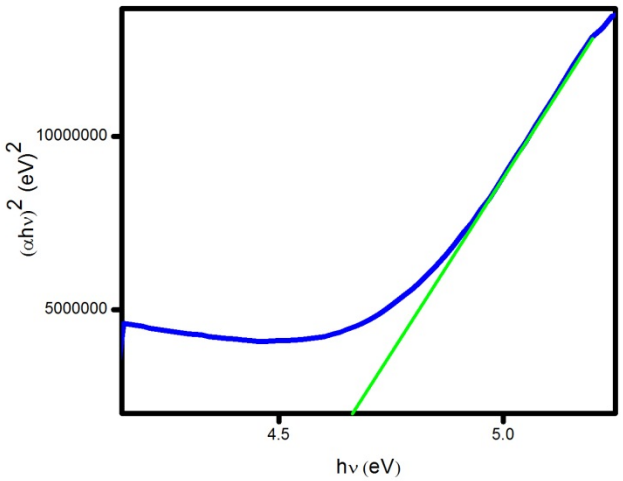

Fig. 6. Tauc's plot of ZrO2

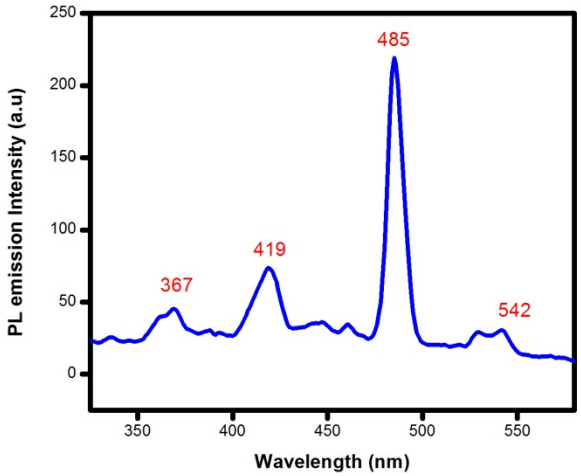

Fig. 7. PL spectra of ZrO2 nanoparticles

using the formula,

$$\alpha = \frac{2.303 \log\left(\frac{1}{T}\right)}{t} \quad (2)$$

Here, 'T' represents transmittance and't' represents the thickness of the sample []. The Tauc plot is drawn to determine the bandgap of ZrO_2 and it is shown in Fig. 6. It is identified that, the variation of $(\alpha h\vartheta)^2$ with respect to $h\vartheta$ is linear which reveals the transition that is directly allowed. The bandgap energy of the ZrO_2 nanoparticle found to be 4.6 eV.

oluminescence analysis

Photoluminescence investigations provide a study on electrical characterization and discrete electronic states. PL emission spectra can be used for the analysis of surface, interface, and impurity levels of nanoparticles [33]. The PL analysis offers fine points on the effect of the transfer of charge and the recombination of electron and hole-pair on the photocatalytic nanoparticle. The luminescence of ZrO_2 occurs due to the transition of electrons from the valence band to the conduction band while a new energy level is formed at the surface of the ZrO_2 nanoparticles [31]. Fig. 7 shows the PL emission spectra of ZrO_2 nanoparticles with an excitation wavelength of 270nm. It is observed that the emission peaks obtained at 367nm in the UV region and 419nm, 485nm, 542nm are in the visible region. The peak centered in the UV region is due to the near band edge transition because of

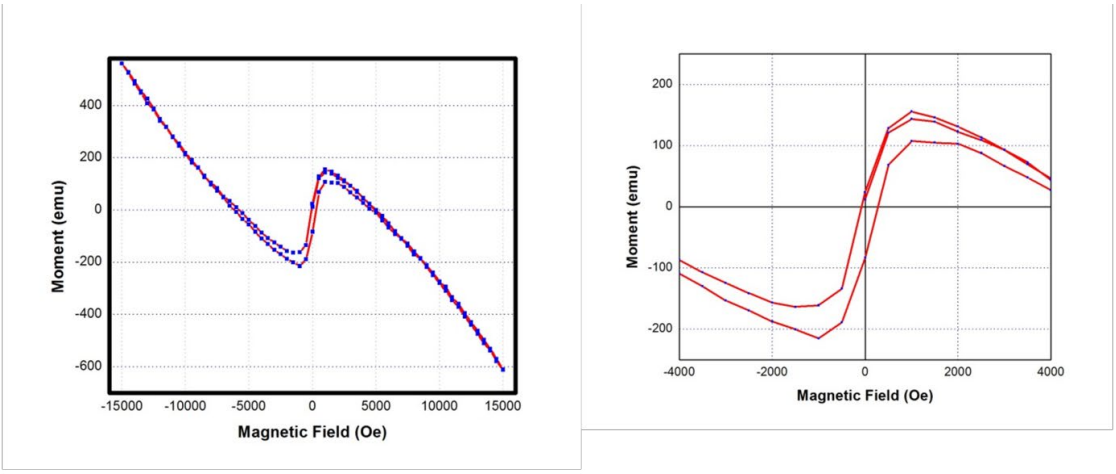

Fig. 8. VSM analysis of ZrO2 nanoparticles

the free excitons recombination. The peak centered in the visible region is due to the occupation of electrons in the mid-band gap trap states such as oxygen vacancies and surface defects [32]. Thus the photoluminescence analysis elucidates that the luminescence of ZrO_2 nanoparticles is due to the oxygen surface defects and vacancies.

Magnetic Properties

The magnetic properties of ZrO2 nanoparticles are analyzed using Vibrating Sample Magnetometer (VSM) at room temperature with a maximum field of 15000 Oe. Fig. 8 shows the obtained M-H loop. The parameters of the M-H loop such as coercivity (Hci), saturation magnetization (M_s), and remanence magnetization (M_r) are observed from the loop.

The observed value of coercivity (Hci) is 2535.6 Oe, saturation magnetization (M_s) is 586.89 × 10^{-6} emu/gm and remanence magnetization (M_r) is 53.525 × 10^{-6} emu. The hysteresis loop shows perfect Room Temperature Ferromagnetism (RTFM). A similar M-H loop has been observed earlier for ferromagnetism [34,35]. Since the coercivity of the prepared ZrO2 nanoparticle is high, it is observed that the ZrO2 nanoparticle is a hard ferromagnetic material. It requires more magnetic fields to demagnetize the material. In the absence of a magnetic field for a certain duration, there will be a magnetic effect in the material and it is called permanent magnetic materials. It is widely used in different fields such as telecommunication, data processing, electronics, and instrumentation. The occurrence of RTFM is due to the presence of oxygen vacancies and surface defects as a result of the large surface energy volume ratio for nano-sized particles. The interface amongst Zr ions is due to this oxygen vacancy. PL measurements reveal the confirmation of oxygen vacancies. The tetrahedral position is occupied by oxygen ions of tetragonal ZrO_2. Due to this a model of defect structure is created. For charge compensation, two Zr^{3+} ions are formed for one oxygen vacancy [30].

Thermal analysis

The thermal behavior of ZrO_2 nanoparticles is analyzed using Thermogravimetric (TG) and Differential Thermal Analysis (DTA) studies under Nitrogen gas atmosphere. Fig. 9 shows the TG / DTA curve of ZrO_2 nanoparticles.

It is found that there is an abrupt reduction of weight loss at 70°C and there is a gradual weight loss with respect to an increase of temperature after 500°C. This abrupt reduction of loss is owing to the defeat of moisture in the synthesized material [35]. The DTA graph shows the endothermic peak at 405°C in which maximum heat is absorbed in the synthesized material. The weight loss at 70°C may be due to the trapped moisture and acetate in the sample and the weight loss after 500◦C may be due to the organic residues.

Photocatalytic Activity

The photocatalytic performance of the prepared catalyst ZrO_2 has experimented with the degradation of methylene blue (MB) organic dye. An aqueous solution of methylene blue (0.1M, 50ml) is taken and 0.2g of photocatalyst zirconia is added. The experiment is done under UV light irradiation. The solution is exposed to a halogen

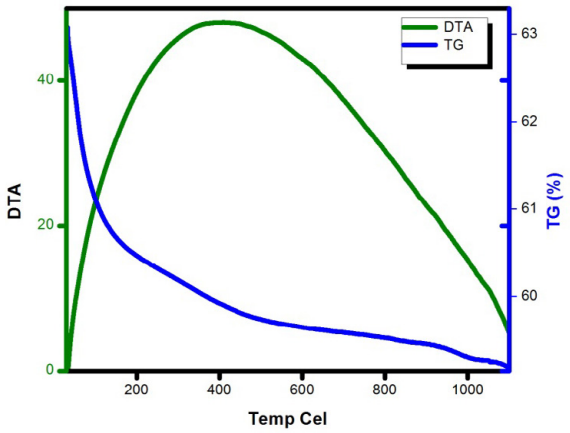

Fig. 9. TG / DTA curve of ZrO2 nanoparticles

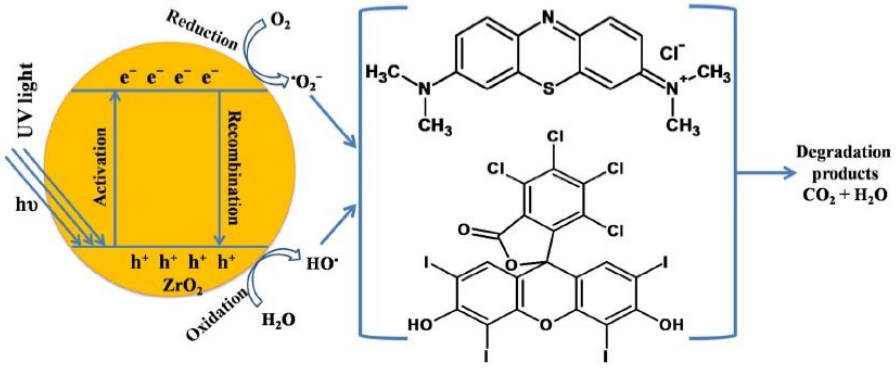

Fig. 10. Photocatalytic degradation mechanism of ZrO2 nanoparticles

lamp of 50W with continuous stirring. For every 60 min, 4 ml of dye solution is taken from the system and the degradation percentage is analyzed by UV-Vis spectrometer.

Photodegradation mechanism

The electrons from the valance band move to the conduction band Under UV light irradiation. Due to this movement of electrons, holes are generated in the valance band and free electrons are generated in the conduction band. H_2O and O_2 from the moisture react with holes in the valance band and electrons in the conduction band, thus produces hydroxyl radical and superoxide radical [36]. These radicals react with the MB organic dye and provide degradation products. The degradation mechanism is shown in Fig. 10.

The following equations provide the detail of the degradation mechanism.

$$ZrO_2 + h\vartheta \rightarrow ZrO_2\left(e_{CB}^- + h_{VB}^+\right)$$

$$ZrO_2(e_{CB}^-) + O_2 \rightarrow ZrO_2 + O_2^{\cdot}$$

$$H_2O \rightarrow H^+ + OH^{\cdot}$$

$$^{\cdot}O_2 + H^- \rightarrow {}^{\cdot}HO_2$$

$$ZrO_2(e_{CB}^-) + {}^{\cdot}HO_2 + H^+ \rightarrow H_2O_2$$

$$ZrO_2\left(h_{VB}^+\right) + Dye \rightarrow Degradation\ products$$

$$HO_2^- + H^+ \rightarrow H_2O_2$$

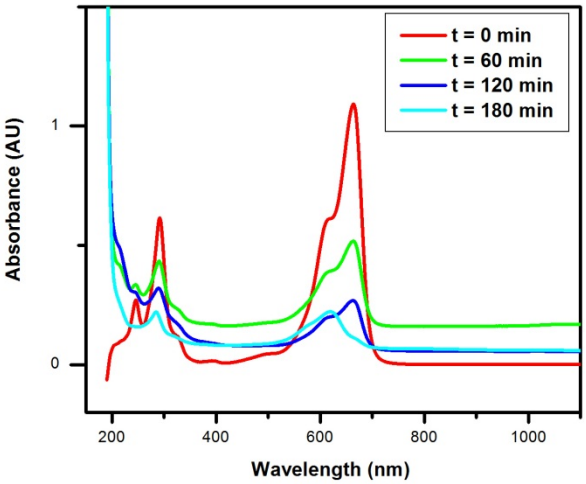

Fig. 11. Optical absorbance spectra of MB dye using ZrO2

$$HO_2^{\cdot} + e^{-} \rightarrow HO_2^{-}$$

Hydroxyl radical $(^{\cdot}OH)$ and superoxide radical $(O_2^{\cdot})$ are involved in the degradation of MB organic dye.

Photocatalytic degradation of MB

The optical absorbance spectra of the degradation of methylene blue (MB) dye using Zirconia are shown in Fig. 11. From the absorbance spectrum, the strong peak is identified at 663.25 nm which is the absorption wavelength of methylene blue (MB) dye. The following equation provides the removal efficiency (E) of MB degradation,

$$E = \frac{C_0 - C}{C_0} \times 100 \ \% \qquad (3)$$

where $C_0 is$ the initial concentration of dye and C is the concentration of MB after UV irradiation. It is observed that 53% of methylene blue (MB) dye is degraded after 1 hour and 80% of methylene blue (MB) dye is degraded after 3 hours. This is mainly due to the high crystallinity nature of t-ZrO_2 prepared at 500°C, small crystallite size, and well-defined morphology and surface properties. The normalized residual concentration of MB dye is estimated using $C_t / C_o = A_t / A_o$, where C_o and C_t are the initial and residual concentrations of MB dye [25]. A_t and A_o are the absorbance intensity at time t and at time t = 0 obtained from the UV-absorbance spectrum.

The growth of the rod-shaped particle is greater in one direction with respect to the growth of the particle in other dimensions [26]. Since the morphology of the prepared nanoparticle is rod shape, the surface area of the particle is high. The high surface area provides more active sites for the reaction of photodegradation [27]. XRD analysis clearly shows that the high crystalline nature of the prepared catalyst thus produces active oxygen sites which may act as scattering centers for the combination of electron-hole pairs. Due to this property, the efficiency of the degradation of MB is high for zirconia even though it has a wide bandgap. The decomposition of MB dye by ZrO_2 with respect to time is shown in Fig. 12. The concentrations of MB dye with and without adding ZrO2 nanoparticles are shown in the graph. We find that the photocatalytic activity of the prepared ZrO_2 nanoparticles provides better results when compared to the previously reported results [11, 37]. The removal percentage of MB dye with different catalysts is presented in Table 1.

Anti-bacterial and Anti-fungal assessment

Synthesized nano zirconia rods are screened for their antibacterial activity against gram-negative pathogens such as *E.coli*, *pseudomonas aeruginosa*, and gram-positive pathogens such as *Bacillus cereus*, *Staph aureus*. Also, the antifungal activity against *Candida albicans* and *Candida parapsilosis* are studied by the Kirby-Bauer test. The antimicrobial activity of nanoparticles is related to the electromagnetic attraction between the positively charged nanoparticles and negatively charged microbes. During this attraction, microbes

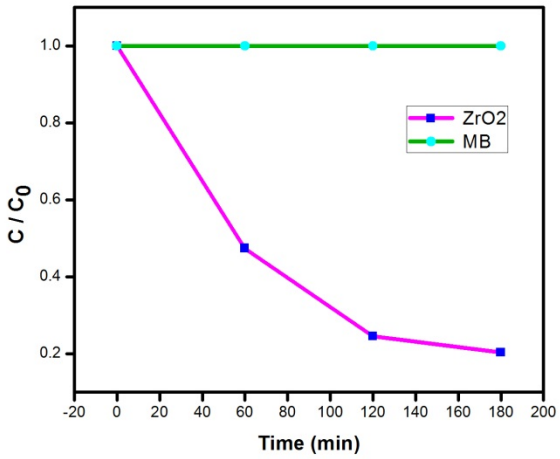

Fig. 12. The removal efficiency of ZrO2

Table 1. Comparison of photocatalytic activity of different catalysts

Light Source	Catalyst preparation method	Catalyst	Irradiation time (min)	Degradation efficiency (%)	Reference
Visible light	Facile hydrothermal	SnS_2	100	62	[39]
Visible light	Sol-gel	TiO_2	180	72.4	[27]
UV	Sol-gel	TiO_2	180	80	[38]
UV	Sol-gel	ZrO_2	60	34	[37]
UV	Co-precipitation	ZrO_2	180	80	Proposed

Table 2. Anti-bacterial and Anti-fungal assessment of ZrO2

Sample	Anti-bacterial Assessment				Antifungal assessment	
	Gram Positive		Gram Negative			
	Bacillus cereus (mm)	Staph aureus (mm)	Escherichia coli (mm)	Pseudomonas aeruginosa (mm)	Candida albicans (mm)	Candida parapsilosis (mm)
Amikacin	16	15	21	37	NA	NA
t-ZrO_2	27	28	26	28	25	18
Nystatin	NA	NA	NA	NA	20	15

get oxidized and destroyed [35].

The results obtained for the antibacterial and antifungal activities are summarized in Table 2. Fig. 13 (a-d) shows the inhibition zones of antibacterial and Fig. 13 (e,f) shows the inhibition zones of antifungal activity. These results reveal that the prepared Zirconia holds superior antimicrobial activity. ZrO_2 nanoparticle has reactive oxygen species and it behaves well as an antibacterial agent. Based on XRD and SEM analysis, Zirconia is chosen for antibacterial screening. Small-sized zirconia nanoparticles are allowed to attach to the cell wall of bacteria and they easily penetrate it, which may improve their anti-bacterial activity.

It is observed that the synthesized ZrO_2 nanoparticles obtain better inhibition against *Pseudomonas aeruginosa* in gram-negative and *Staphaureus* in gram-positive. The inhibition capability of nano zirconia rods is compared with Amikacin. The results reveal that ZrO_2 nanoparticles act better antibacterial activity against E.coli in gram-negative and both *Bacillus cereus* and *Staphaureus* in gram-positive. Zirconia exhibits a greater potential in killing the bacterial strains due to its high surface area. The reason for the superior effect against bacterial strains of ZrO_2 nanoparticles may be the active oxygen species that make the particle accumulate or deposit on the bacterial cells to prevent the growth. The growth of the bacterial cell can be struck by the accumulation of nanoparticles in the bacterial membrane and cytoplasmic region of the cells. The accumulation

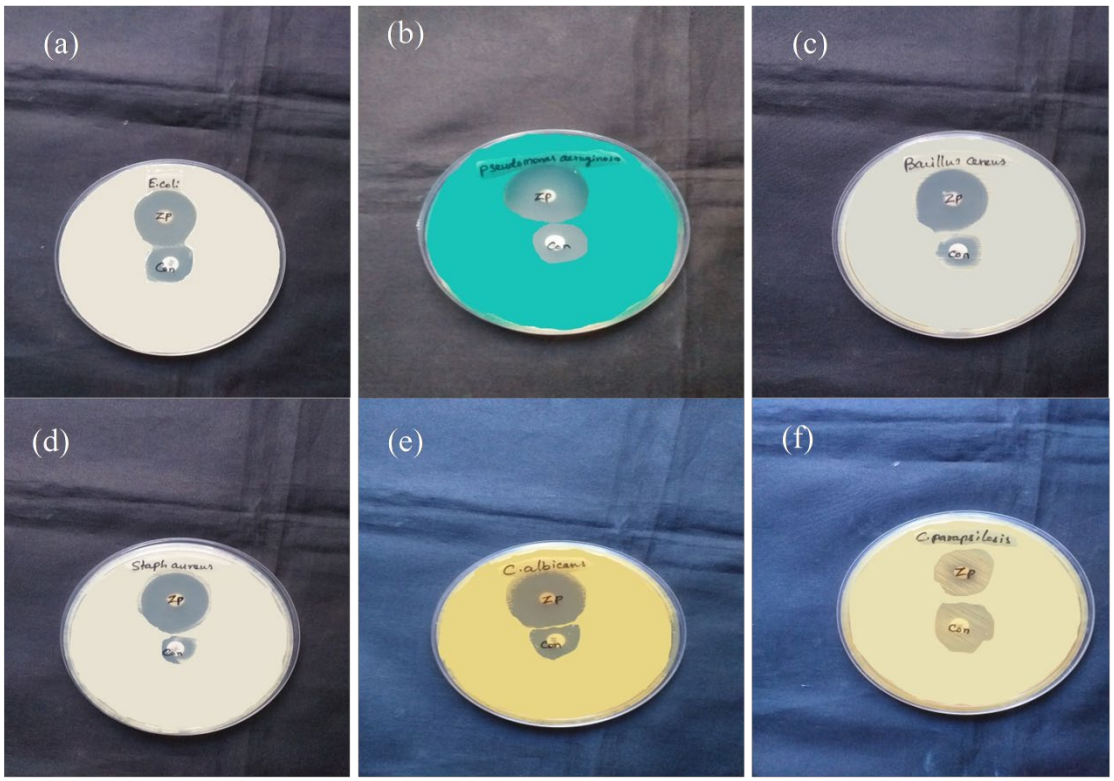

Fig. 13. Inhibition zones of bacterial and fungal strains

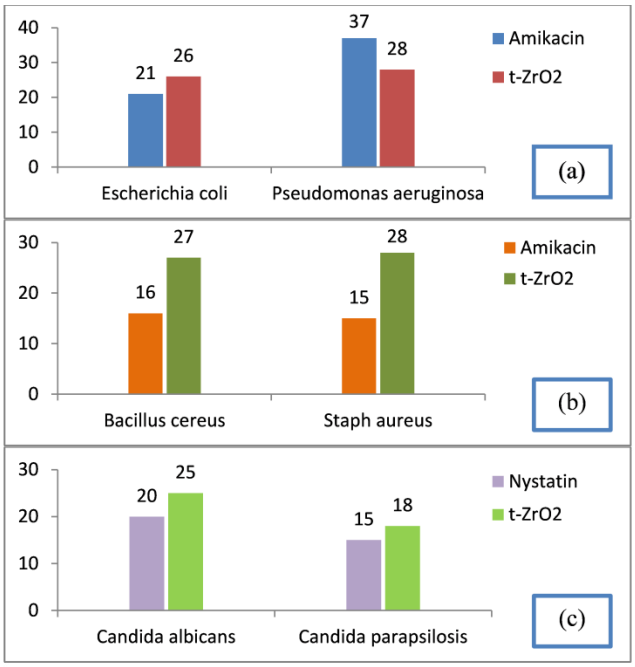

Fig. 14. Antibacterial and Antifungal activity of Zirconia

of nanoparticles is accomplished by increasing the permeability of the cell wall [36].

The antifungal images of Zirconia nanoparticles shown in Fig. 13(e,f) reveal better results against antifungal strains such as *Candida albicans* and *Candida parapsilosis*. The inhibition capability of nano zirconia rods is compared with Nystatin. Fig. 14 shows the performance of ZrO_2 for antimicrobial activities in comparison with the antimicrobial agents. A comparison of the antifungal activity data of the test compound against fungal strains indicates that the test compound is more active against Nystatin to kill both the *Candida albicans* and *Candida parapsilosis*. Generally, the chemical reactivity of nanocrystallites depends on their shapes, atomic arrangement of the surface, and surface energy [9]. The surface energy is an important parameter of the nanoparticle to define the antibacterial and antifungal activity. Since the prepared nano Zirconia has rod shape morphology, it has a high surface area and high surface energy. Due to this high surface energy, the prepared nano has better antimicrobial activity.

CONCLUSION

Tetragonal zirconia has been synthesized by the simple co-precipitation method. The synthesized Zirconia has been characterized by various characterization methods such as XRD, SEM, EDX, UV-Vis, PL, VSM, and TG/DTA analysis. The XRD analysis indicates that the average crystallite size is 29.74nm and SEM analysis depicts rod-shaped morphology. The Ferromagnetic behavior is found using VSM measurements. The performance of Zirconia nanorods in various applications such as photocatalysis, anti-bacterial and anti-fungal activities has been analyzed. t-ZrO_2 photocatalyst degrades methylene blue dye with 80% removal efficiency in 180 minutes. The antibacterial activity of the synthesized Zirconia has experimented against *Escherichia coli*, *Pseudomonas aeruginosa*, *Bacillus cereus*, and *Staphaureus*. The antifungal activity of the synthesized Zirconia has experimented against *Candida albicans* and *Candida parapsilosis* using the Kirby-Bauer test. t-ZrO_2 shows a superior inhibiting effect against both gram-positive and gram-negative bacterial pathogens Owing to its high surface area, it exhibits the greatest inhibiting effect against fungal strain.

CONFLICTS OF INTEREST

The authors declare that there are no conflicts of interest regarding the publication of this paper.

REFERENCES

1.V. John, Spirig, High-temperature zirconia oxygen sensor with sealed metal/metal oxide internal reference.Sensors and Actuators B: Chemical, **124** 1 (2007) 192-201.

2. Panda D, Tseng T-Y. Growth, dielectric properties, and memory device applications of ZrO2 thin films. Thin Solid Films. 2013;531:1-20.

3.David Cooper, Gina Golledge, Influence of calcination temperature on structural, optical, dielectric properties of nano zirconium oxide, Optik, 127 11 (2016) 4889-4893.

4. Yamaguchi T. Application of ZrO2 as a catalyst and a catalyst support. Catalysis Today. 1994;20(2):199-217.

5. Xiao M, Li Y, Lu Y, Ye Z. Synthesis of ZrO2:Fe nanostructures with visible-light driven H2 evolution activity. Journal of Materials Chemistry A. 2015;3(6):2701-6.

6. Jiang W, He J, Zhong J, Lu J, Yuan S, Liang B. Preparation and photocatalytic performance of ZrO2 nanotubes fabricated with anodization process. Applied Surface Science. 2014;307:407-13.

7. Marcos FCF, Assaf JM, Giudici R, Assaf EM. Surface interaction of CO2/H2 mixture on mesoporous ZrO2: Effect of crystalline polymorph phases. Applied Surface Science. 2019;496:143671.

8. Zhang D, Zeng F. Structural, photochemical and photocatalytic properties of zirconium oxide doped TiO2 nanocrystallites. Applied Surface Science. 2010;257(3):867-71.

9. Wang X, Wu H-F, Kuang Q, Huang R-B, Xie Z-X, Zheng L-S. Shape-Dependent Antibacterial Activities of Ag2O Polyhedral Particles. Langmuir. 2009;26(4):2774-8.

10.Gu FX, Karnik R, Wang AZ, Targeted nanoparticles for cancer therapy. *Nano Today*., 3 (2007) 14–21.

11. Zheng H, Liu K, Cao H, Zhang X. l-Lysine-Assisted Synthesis of ZrO2 Nanocrystals and Their Application in Photocatalysis. The Journal of Physical Chemistry C. 2009;113(42):18259-63.

12.Jangra SL, Stalin L, Dilbaghi N, Antimicrobial activity of zirconia (ZrO2) nanoparticles and zirconium complexes. J Nanosci Nanotechnol., 12 9 (2012) 7105–7112.

13. Veeraapandian S, Sawant SN, Doble M. Antibacterial and Antioxidant Activity of Protein Capped Silver and Gold Nanoparticles Synthesized with *Escherichia coli*. Journal of Biomedical Nanotechnology. 2012;8(1):140-8.

14. Huang Z, Li F, Jiao C, Liu J, Huang J, Lu L, et al. Molten salt synthesis of La2Zr2O7 ultrafine powders. Ceramics International. 2016;42(5):6221-7.

15.D. Prusty, A. Pathak, A. Chintha, Structural investigations on the compositional anomalies in lanthanum zirconate system synthesized by coprecipitation method. J. Am. Ceram. Soc. 97 (2014) 718-724.

16. Nirmal M, Brus L. Luminescence Photophysics in Semiconductor Nanocrystals. Accounts of Chemical Research. 1998;32(5):407-14.

17. Rockenberger J, Scher EC, Alivisatos AP. A New Nonhydrolytic Single-Precursor Approach to Surfactant-Capped Nanocrystals of Transition Metal Oxides. Journal of the American Chemical Society. 1999;121(49):11595-6.

18. Zhang J, Qin W, Zhang J, Wang Y, Cao C, Jin Y, et al. A Novel Approach from Infrared to Ultraviolet Emission Enhancement in Yb3+, Er3+:CaF2 Nanofilms. Journal of Nanoscience and Nanotechnology. 2008;8(3):1258-60.

19.S. Sugi, S. Radhika& C. M. Padma, Antimicrobial Activity of PVA Mediated Zincstrontium Ferrite Composites, Journal of Shanghai Jiaotong University, **16** 11 (2020) 396-403.
20. Gowri S, Rajiv Gandhi R, Sundrarajan M. Structural, Optical, Antibacterial and Antifungal Properties of Zirconia Nanoparticles by Biobased Protocol. Journal of Materials Science & Technology. 2014;30(8):782-90.
21. Job CB, Shabu R, Paulraj S. Growth, structural, optical, and photo conductivity studies of potassium tetra fluoro antimonate crystal. Optik. 2016;127(8):3783-7.
22.X. Wang, H. F. Wu, Q. Kuang, R. B. Huang, Z. X. Xie, and L. S. Zheng, Langmuir, Antibacterial Properties of Novel Bacterial Cellulose Nanofiber Containing Silver Nanoparticles. Chinese Journal of Chemical Engineering, 26 2774 (2010).
23.S.Radhika, C.M. Padma, S.Ramalingom, T.ChithambaraThanu, Growth, optical, thermal, mechanical and dielectric studies of potassium sulphate crystals doped with urea, Archives of Physics Research, **4** 1 (2013) 49-59.
24. Sadeghzadeh-Attar A. Efficient photocatalytic degradation of methylene blue dye by SnO2 nanotubes synthesized at different calcination temperatures. Solar Energy Materials and Solar Cells. 2018;183:16-24.
25.J.R.Sheeba, S.Radhika and C.M.Padma, Photo catalytic degradation of Methylene Blue Dye by Cu doped SnO_2Nano Crystals, J. Wutan Huatan Jisuan Jishu **16** 9 (2020) 66-76.
26. Ahmed B, Kumar S, Kumar S, Ojha AK. Shape induced (spherical, sheets and rods) optical and magnetic properties of CdS nanostructures with enhanced photocatalytic activity for photodegradation of methylene blue dye under ultra-violet irradiation. Journal of Alloys and Compounds. 2016;679:324-34.
27. Sankar KV, Ashok M. Significantly enhanced photo catalytic activities of PbBi2Nb2O9(Bulk)/TiO2(Nano) hetero structured composites for methylene blue dye degradation under visible light. Materials Chemistry and Physics. 2020;244:122659.
28. French RH, Glass SJ, Ohuchi FS, Xu YN, Ching WY. Experimental and theoretical determination of the electronic structure and optical properties of three phases ofZrO2. Physical Review B. 1994;49(8):5133-42.
29. Reddy CV, Babu B, Reddy IN, Shim J. Synthesis and characterization of pure tetragonal ZrO2 nanoparticles with enhanced photocatalytic activity. Ceramics International. 2018;44(6):6940-8.
30. Kumar S, Bhunia S, Singh J, Ojha AK. Absence of room temperature ferromagnetism in Fe stabilized ZrO2 nanostructures and effect of Fe doping on its structural, optical and luminescence properties. Journal of Alloys and Compounds. 2015;649:348-56.
31. Arjun A, Dharr A, Raguram T, Rajni KS. Study of Copper Doped Zirconium Dioxide Nanoparticles Synthesized via Sol–Gel Technique for Photocatalytic Applications. Journal of Inorganic and Organometallic Polymers and Materials. 2020;30(12):4989-98.
32. Horti NC, Kamatagi MD, Nataraj SK, Wari MN, Inamdar SR. Structural and optical properties of zirconium oxide (ZrO2) nanoparticles: effect of calcination temperature. Nano Express. 2020;1(1):010022.
33. Gfroerer TH. Photoluminescence in Analysis of Surfaces and Interfaces. Encyclopedia of Analytical Chemistry: John Wiley & Sons, Ltd; 2006.
34. Singh G, Pawan, Singh A, Shilpy, Diksha, Suman, et al. Propargyl-functionalized single arm allied Anthracene based Schiff bases: Crystal structure, solvatochromism and selective recognition of Fe3+ ion. Journal of Molecular Structure. 2021;1229:129618.
35. Etape EP, Foba-Tendo J, Ngolui LJ, Namondo BV, Yollande FC, Nguimezong MBN. Structural Characterization and Magnetic Properties of Undoped and Ti-Doped ZnO Nanoparticles Prepared by Modified Oxalate Route. Journal of Nanomaterials. 2018;2018:1-9.
36. Karthik K, Madhukara Naik M, Shashank M, Vinuth M, Revathi V. Microwave-Assisted ZrO2 Nanoparticles and Its Photocatalytic and Antibacterial Studies. Journal of Cluster Science. 2018;30(2):311-8.
37. Ratnayake SP, Mantilaka MMMGPG, Sandaruwan C, Dahanayake D, Murugan E, Kumar S, et al. Carbon quantum dots-decorated nano-zirconia: A highly efficient photocatalyst. Applied Catalysis A: General. 2019;570:23-30.
38. Barakat MA, Schaeffer H, Hayes G, Ismat-Shah S. Photocatalytic degradation of 2-chlorophenol by Co-doped TiO2 nanoparticles. Applied Catalysis B: Environmental. 2005;57(1):23-30.
39. Balu S, Uma K, Pan G-T, Yang T, Ramaraj S. Degradation of Methylene Blue Dye in the Presence of Visible Light Using SiO2@α-Fe2O3 Nanocomposites Deposited on SnS2 Flowers. Materials. 2018;11(6):1030.